ACS NANO

www.acsnano.org

ARTICLE

# Quasi-Solid-State Conversion with Fast Redox Kinetics Enabled by a Sulfonamide-Based Electrolyte in Li−Organic Batteries

Huang Cai, Xinke Cui, Yonghao Shi, Yuxin Zhang, Xinran Chen, Linghan Fan, Jian Zhou, Chuanjin Tian,* and Weijiang Xue*

Cite This: *ACS Nano* 2024, 18, 32723−32731

Read Online

ACCESS | Metrics & More | Article Recommendations | Supporting Information

**ABSTRACT:** **The serious dissolution of organic electrode materials (e.g., perylene-3,4,9,10-tetracarboxylic dianhydride, PTCDA) in electrolytes is a major challenge, deteriorating their electrochemical performances and hindering the interpretation of the fundamental redox reaction mechanisms including the intrinsic kinetics and the solvent cointercalation. To address these issues, we propose a rationally designed sulfonamide-based electrolyte to enable a quasi-solid-state conversion (QSSC) of the PTCDA cathode by effectively suppressing its dissolution in the electrolyte. Benefiting from the QSSC, the Li||PTCDA cells can retain ∼95.8% of the original capacity after 300 cycles with both high and stable energy efficiencies >95%, even comparable to the layered transition-metal oxide cathodes, greatly outperforming an ether-based electrolyte with a high PTCDA solubility. The high energy efficiencies indicate that the QSSC of PTCDA has intrinsic fast redox kinetics. Furthermore, the solvent cointercalation mechanism was investigated by density functional theory/molecular dynamic calculations. This work develops a strategy for designing electrolytes for highly stable and efficient Li−organic batteries.**

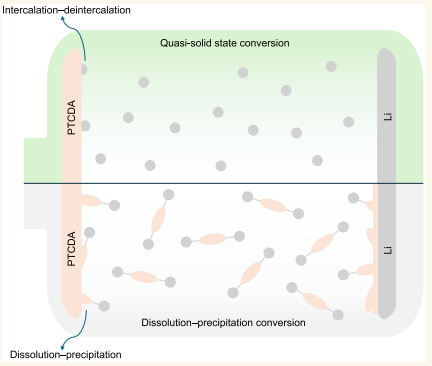


**KEYWORDS:** *PTCDA, fast redox kinetics, sulfonamide-based electrolyte, Li−organic batteries, quasi-solid-state conversion, energy efficiency*

## INTRODUCTION

Organic electrode materials (OEMs)[1] have become increasingly attractive since they can decouple the dependency of lithium-based[2,3] batteries on transition metals.[4] Among all of the well-studied OEMs, perylene-3,4,9,10-tetracarboxylic dianhydride (PTCDA),[5,6] featuring the molecular structure composed of perylene and peripherally rich oxygen atoms (Figure 1a), is one of the promising candidates for future applications. However, it still faces major challenges for most OEMs, the serious dissolution in organic electrolytes and its related shuttling issue when matching the very reactive lithium−metal anodes[7] (LMAs). It eventually deteriorates the cycling performance and Coulombic efficiency (CE), though such a Li||PTCDA architecture can maximize the cell energy density. More importantly, the redox reaction mechanism of the PTCDA upon Li intercalation and deintercalation has been made quite complicated since the dissolution−precipitation process (Figure 1b) is involved, as extra energy is needed for overcoming the nucleation barrier during precipitation and "reluctantly" for keeping the dissolved redox mediators (RMs, in a solubilized form written as $PTCDA^{\alpha-}$−electrolyte, Figure 1b) moving between the cathode and the anode. In this scenario, mechanistic studies of the intrinsic redox reaction mechanism are hampered. Therefore, to benefit both the cell performance and the fundamental research, an ideal scenario is to invoke a (quasi-)solid-state[8] conversion (QSSC, Figure 1c) for the PTCDA cathode.

For a QSSC without the active material dissolution, one may first wonder if it would lead to a low utilization of the active material and sluggish redox kinetics, which is the case for Li−S batteries[9−11] since the dissolution is essential for activating the electrical insulator $S_8$ (conductivity: $5 \times 10^{-30}$ S cm$^{-1}$).[12] For comparison, in principle, such dissolution should not be necessary for PTCDA due to its high electric conductivity

Received: July 30, 2024
Revised: October 29, 2024
Accepted: November 5, 2024
Published: November 13, 2024







https://doi.org/10.1021/acsnano.4c10343
*ACS Nano* 2024, 18, 32723−32731

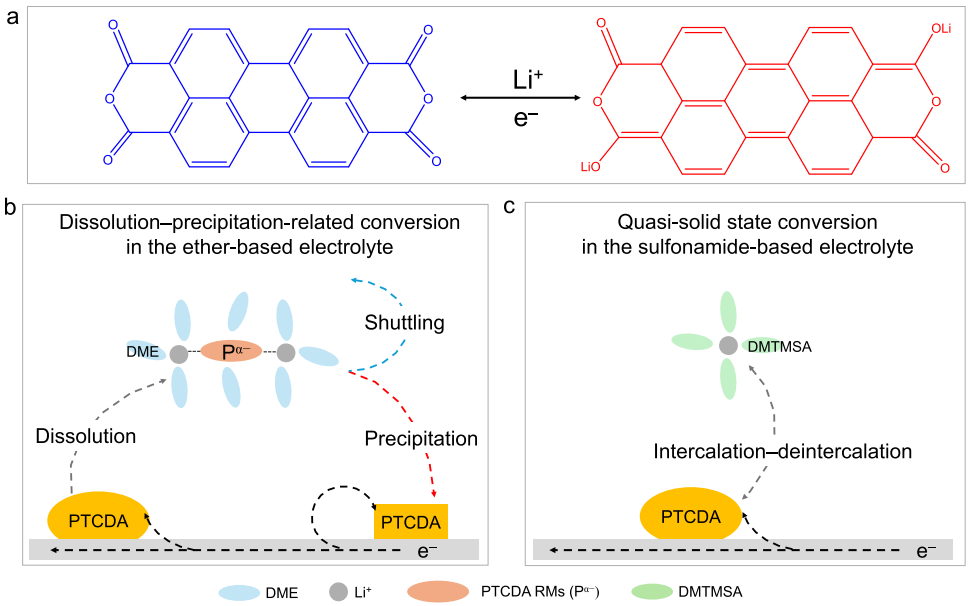


**Figure 1. Schematic illustration of the reaction mechanisms of the PTCDA cathodes. (a) Proposed reversible Li intercalation−deintercalation process in PTCDA, corresponding to a specific capacity of ∼137 mAh $g^{-1}$. (b) Dissolution and precipitation process of PTCDA in the ether-based electrolytes, which can dissolve PTCDA RMs ($P^{\alpha-}$). The solvated $P^{\alpha-}$ anions can diffuse to and "poison" the reactive LMA ("shuttling effect"). During discharging, they need to overcome the nucleation barrier and deposit elsewhere other than the original states. (c) Proposed quasi-solid-state conversion can be enabled in a weakly solvated *N,N*-dimethyl-trifluoromethanesulfonamide-based electrolyte involving the intercalation−deintercalation reaction with suppressing the shuttling effect.**

ranging from $10^{-3}$ (nanowire) to $10^{-6}$ (film) S $cm^{-1}$[13] (at the similar level as the $LiMn_2O_4$ and $LiCoO_2$[14]) due to the $\pi-\pi$ conjugation between the layer-stacked molecules. Consequently, we can decouple the dissolution behavior and its effect on the electrochemical performance in the Li||PTCDA cell by realizing the QSSC, which is the basis for simplifying the redox reaction mechanism and for further improving cell performance. On the one hand, for the fundamental research, the ion−solvent cointercalation chemistry[15] has been discovered in layered materials with weak interlayer van der Waals interactions, for example, $Li^+$−propylene carbonate,[16] $Na^+$−ether,[17] and $Ca^{2+}$−dimethylacetamide[18] cointercalating into graphite. For the layered PTCDA cathode, although the cointercalation of methyl viologen cations and hydronium ($H_3O^+$) has been reported,[19] it still remains unclear if the cointercalation occurs in other ion−solvent systems. On the other hand, round-trip energy efficiency [EE, = CE × voltage efficiency (VE)] of the Li||PTCDA cell, an important parameter for practical applications but often neglected in laboratory research,[14] should be introduced to evaluate the redox reaction since the CE and VE are directly associated with the shuttling effect and the redox kinetics during the charging−discharging process, respectively.

Although great progress has been made in suppressing the OEM dissolution by designing various cathode architectures[20,21] to absorb the RMs or by constructing interlayers[22,23] on separators to block the RMs diffusion, these approaches could not tailor the intrinsic solubility of OEMs. Even for the high salt concentration electrolytes (HCEs)[20,24] with minimizing free solvent molecules, there has been an argument for the dependency of salt concentration on RM solubility.[25] Localized high-concentration electrolytes (LHCEs)[26] can effectively weaken the electrolyte polarity by introducing nonpolar components[27] into polar solvents; however, RMs could still be dissolved in the polar components, possibly forming unneglectable diffusion percolation, which may not be ideal for favoring QSSC. Therefore, to avoid such complexity, an effective way for QSSC is to find a single-solvent electrolyte, where the solvent molecules can dissociate lithium salt supporting $Li^+$ conductivity but can sparingly solvate the PTCDA RMs at any state of charge (SOC). At the same time, such an electrolyte should also be compatible with the LMA to achieve good full-cell performance.

In the present work, to realize QSSC in the PTCDA cathode, we select a *N,N*-dimethyl-trifluoromethanesulfonamide (DMTMSA) as the electrolyte solvent,[28] which belongs to the sulfonamide family featuring its high LMA-compatibility.[29] The DMTMSA solvent can dissociate a sufficient amount (1 M) of lithium bis(fluorosulfonyl)imide (LiFSI) to retain a sufficient $Li^+$ conductivity.[28] A single-solvent electrolyte, 1 M LiFSI/DMTMSA, has been yielded, which has a weak solvation capability for the PTCDA molecules. Such a sulfonamide-based electrolyte effectively inhibited the RM dissolution, revealed by multiple visual/postmortem analysis and high CEs of the Li||PTCDA cell, indicating a successful QSSC. High and stable EEs of ∼95% over 300 cycles were also achieved, compared to the steadily decreasing EEs < 90% with an ether-based electrolyte, demonstrating a faster redox kinetics for the QSSC than the traditional dissolution-involved reaction. Furthermore, an excellent cycling performance of ∼95.8% capacity retention after 300 cycles was reached by the sulfonamide-based electrolyte. The density functional theory (DFT) calculations and molecular dynamics (MD) simulations implied that the DMTMSA solvent cointercalation unlikely occurs in the PTCDA bulk, but may be present at the PTCDA−electrolyte interface. This work points toward the fundamental pathway and the electrolyte design strategy for achieving durable and highly efficient Li−organic batteries.


https://doi.org/10.1021/acsnano.4c10343
ACS Nano 2024, 18, 32723−32731

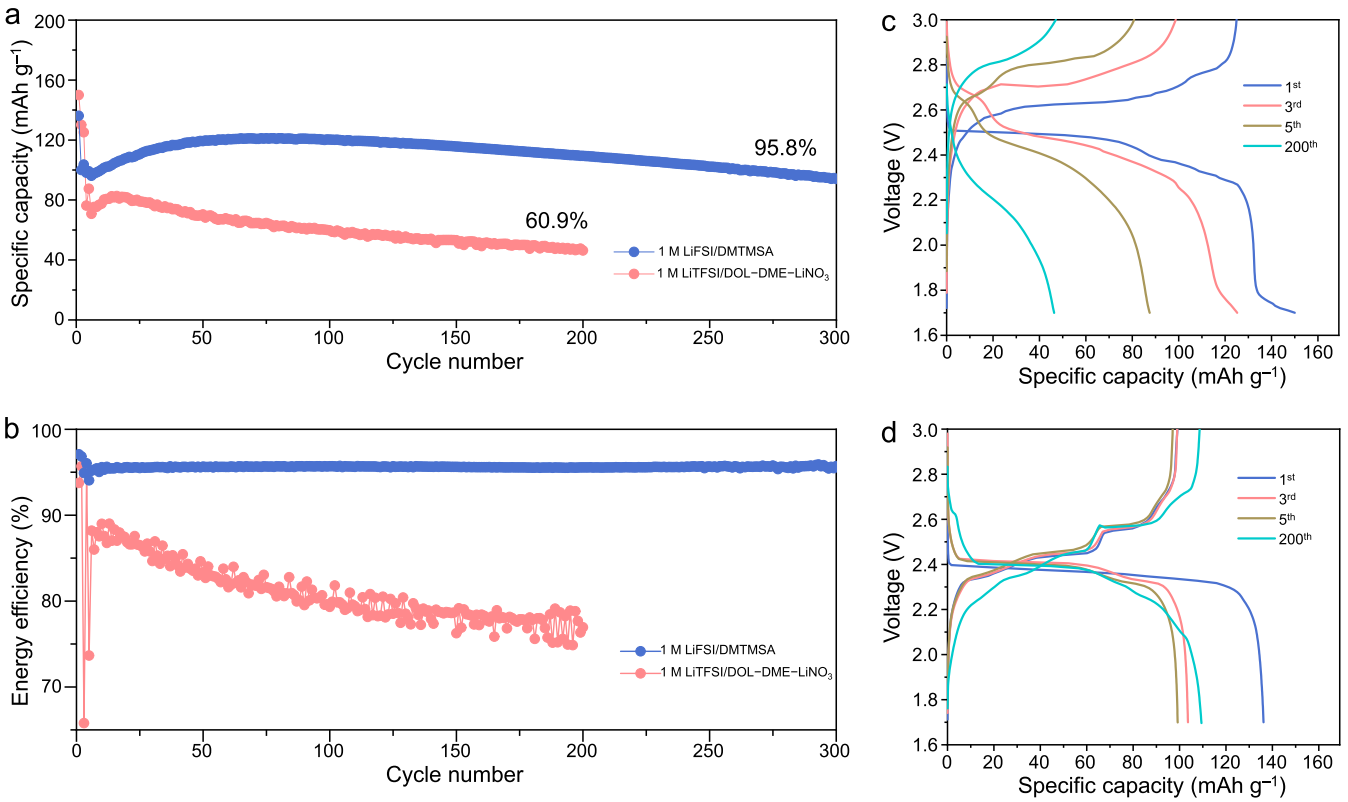


**Figure 2. Electrochemical performances of Li||PTCDA cells using different electrolytes. Specific capacity (a) and energy efficiencies (b) with the investigated electrolytes at 1C (0.1C for the 1st cycle and 0.5C for the 2nd to 3rd cycles). Corresponding voltage profiles of the cells using the ether-based (c) and sulfonamide-based (d) electrolytes.**

## RESULTS AND DISCUSSION

A well-studied ether-based electrolyte,[30] 1 M lithium bis(trifluoromethanesulfonyl)imide (LiTFSI) in 1,2-dimethoxyethane (DME):1,3-dioxolane (DOL) 1:1 (v) with 2 wt % $LiNO_3$ (abbreviated as 1 M LiTFSI/DME-DOL-$LiNO_3$ hereafter), was chosen as the reference electrolyte. It can dissolve the PTCDA RMs to enable the traditional dissolution-involved reaction, but well protecting the LMA by $LiNO_3$ decomposition[31] prior to the PTCDA RMs. Therefore, the effect of LMA on the overpotential and cycling stability during initial cycles can be excluded to make a fair comparison of the intrinsic cathode performances between the ether- and sulfonamide-based electrolytes.

The cycling stability of Li||PTCDA cells was evaluated with 1 M LiFSI/DMTMSA and 1 M LiTFSI/DME-DOL-$LiNO_3$ electrolytes (Figure 2a). With the ether-based electrolyte, the Li||PTCDA cell exhibited a high initial specific capacity of 150 mAh $g^{-1}$ at 0.1C but poor rate performance (87.5 mAh $g^{-1}$ at 1C) and low capacity retention of ~60.9% over 200 cycles. In contrast, the cell with the sulfonamide-based electrolyte delivered an initial capacity of 136 mAh $g^{-1}$ at 0.1C with a higher capacity of ~99.2 mAh $g^{-1}$ at 1C and a much-improved capacity retention of ~95.8% over 300 cycles (Figure 2a). The sulfonamide-based electrolyte also showed more stable CEs of nearly 100% than the fluctuated ones with the reference electrolyte (Supporting Information, Figure S1). More impressively, compared to the steadily decreasing EEs (average ~81.0% over 200 cycles) with the reference electrolyte, stable and high EEs (average ~95.6% over 300 cycles) were achieved (Figure 2b), even surpassing the targeting EEs of 90−95% for $LiNi_xMn_yCo_zO_2$ cathodes.[32] Since the average CEs with both electrolytes are comparable, the large difference in EEs is attributed to the different overpotentials, indicative of much faster redox reaction kinetics of the PTCDA in the sulfonamide-based electrolyte. This can also be reflected by the much smaller gaps between the charging and discharging voltage profiles (Figure 2c,d).

To gain more insight into the kinetics, we conducted galvanostatic intermittent titration technique (GITT) measurements for the cells after 10 cycles. It is noted that the overpotentials of the Li||PTCDA cell cycled in our electrolyte were much smaller than those cycled in the reference electrolyte (Figure 3a). By noticing the different plateaus in voltage profiles in Figure 2c,d, we further deduced the d$Q$/d$V$ plots (Figure 3b,c). The PTCDA cathode with our electrolyte exhibited two sharp reduction peaks at around 2.4 and 2.3 V (Figure 3b), while the one with the reference electrolyte showed multiple reduction gentle peaks with two at 2.5 and 2.7 V (Figure 3c). It is interesting to note that the two-peak characteristics in our electrolyte are also different from the PTCDA in the high-concentration ether-based electrolyte[20] (e.g., 3 M LiTFSI/DOL-DME), which exhibited similar characteristics as the 1 M LiTFSI/DME-DOL-$LiNO_3$ electrolyte but better suppressing the PTCDA RM dissolution. The difference in peak characteristics demonstrates that the redox reaction mechanisms of the PTCDA cathodes in both electrolytes are different, guiding us to carefully study the dissolution behavior of the PTCDA RMs that is mostly associated with the electrolytes.

To visually observe the dissolution behavior, the PTCDA cathodes at fully charged and discharged states in both electrolytes (Figure 3d,e, inset) were immersed in the same


https://doi.org/10.1021/acsnano.4c10343
ACS Nano 2024, 18, 32723−32731

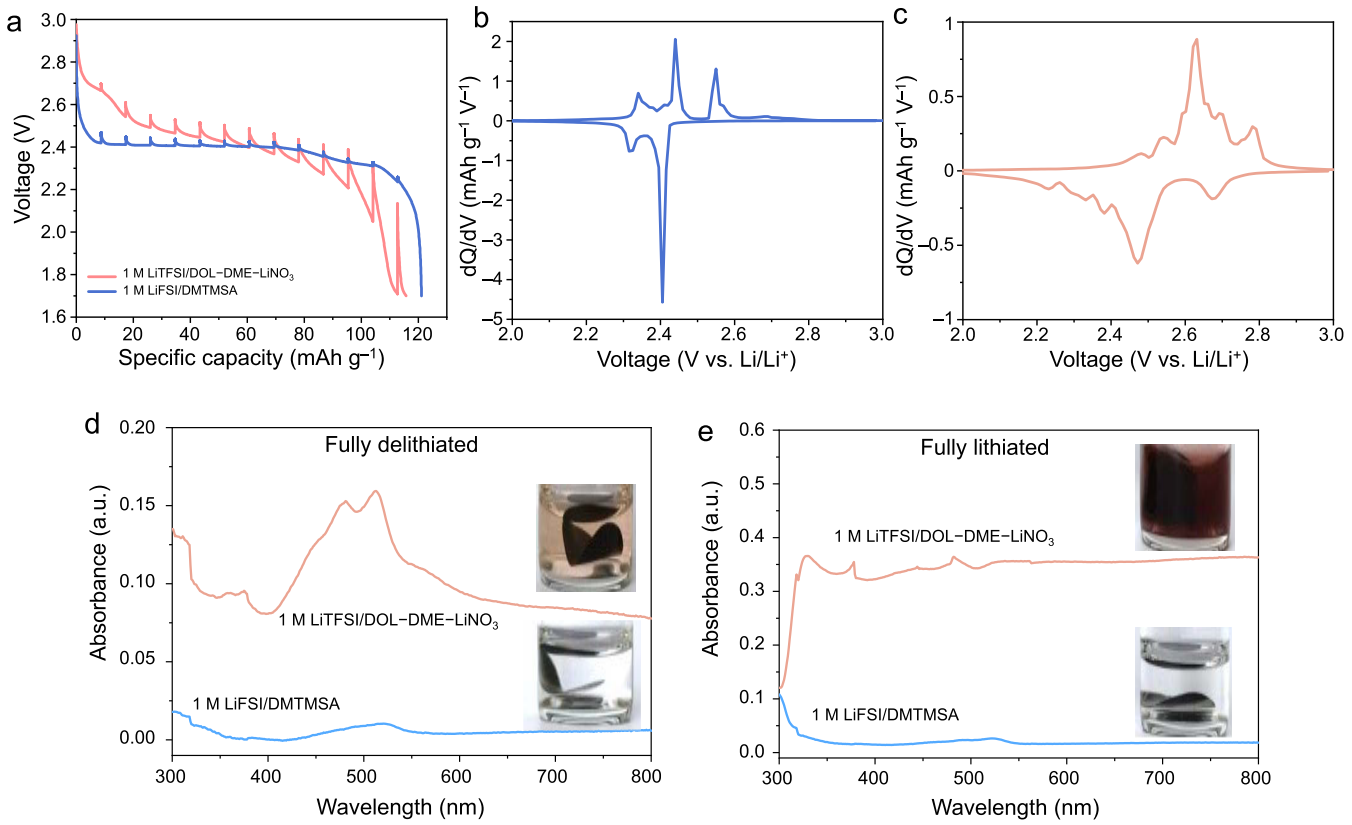


**Figure 3. Electrochemical analysis and dissolution behavior of the PTCDA cathodes in different electrolytes. (a) Discharge voltage profiles of GITT measurements on the cells after 10 cycles in corresponding electrolytes. Corresponding d$Q$/d$V$ profiles of the cells were obtained using 1 M LiFSI/DMTMSA (b) and 1 M LiTFSI/DOL-DME-$LiNO_3$ (c) electrolytes. Visual discrimination (insets) and UV−vis spectra of the PTCDA cathodes at fully delithiated (d) and lithiated (e) states immersed into the corresponding electrolytes for 72 h. The PTCDA cathodes were extracted from the Li||PTCDA cells cycled in both electrolytes for 100 cycles.**

electrolytes for 72 h (more data on the evolution of color change with time shown in Supporting Information, Figure S2). It is apparent that in the ether-based electrolyte, the fully lithiated PTCDA cathode (Figure 3e inset) has a much darker color than the delithiated one (Figure 3d inset), indicating a higher solubility due to the increased polarity by Li intercalation. However, it is intriguing to note that both the PTCDA cathodes at fully lithiated (Figure 3e inset) and delithiated (Figure 3d inset) states showed transparent solutions in the sulfonamide-based electrolyte. The *ex situ* ultraviolet−visible (UV−vis) spectroscopy measurements (Figure 3d,e) demonstrate a much lower absorbance of the 1 M LiFSI/DMTMSA solutions than the 1 M LiTFSI/DME-DOL-$LiNO_3$ solutions, further verifying the much lower solubility of PTCDA RMs in DMTMSA.

To further reveal the impact of electrolytes on the Li|| PTCDA cells, we conducted multiple postmortem analyses on the PTCDA cathodes and the LMAs cycled in different electrolytes. The morphologies of the PTCDA cathodes were investigated by scanning electron microscopy (SEM) (Figure 4a−c and Supporting Information, Figure S3). Brick-like submicron tightly-packed particles with aspect ratios between 3 and 4[33] were observed in the SEM image of the PTCDA cathode before cycling (Figure 4a). After 100 cycles in the sulfonamide-based electrolyte (Figure 4b), only a slight change in shape with a little porosity can be observed, while the one cycled in the ether-based electrolyte showed abundant nanoneedle-like particles with a lot of porosity (Figure 4c). In the ether-based electrolyte, a large amount of PTCDA was dissolved during cycling, which was then consumed by the reaction with the counter-electrode LMA, which is responsible for the large difference in the cathode morphology before and after cycling. In addition, X-ray photoelectron spectroscopy (XPS) measurements were conducted to inspect the surface chemistries of the PTCDA cathodes before and after cycling. Two characteristic peaks corresponding to the C−O and C═O bonding in the PTCDA molecule were noted for the pristine cathode (Figure 4d). New peaks in Figure 4e,f representing the presence of C−O−Li bonding at ∼532.5 eV could be attributed to the lithiated PTCDA. Although the cathodes for inspection were fully charged, there could still be some lithiated PTCDA molecules on the cathode surface. Compared to the cathode cycled in the sulfonamide-based electrolyte (Figure 4e), the one cycled in the ether-based electrolyte (Figure 4f) has a much stronger C−O−Li signal, indicating that more lithiated PTCDA molecules were deposited onto the cathode surface. Besides the cathodes, the LMAs cycled in different electrolytes showed large differences in the morphologies. Uniform and compact Li-metal ($Li^0$) particles were noted for the LMA cycled in the sulfonamide-based electrolyte (Figure 4g and Supporting Information, Figure S4a). For comparison, the one cycled in the ether-based electrolyte showed large nonuniform $Li^0$ agglomerations with a lot of PTCDA floccules (Figure 4h and Supporting Information, Figure S4b), though such an electrolyte is a well-known LMA-compatible electrolyte with uniform $Li^0$ deposition.[34] It demonstrates that the dissolved PTCDA RMs shuttling to the LMA surface affect the $Li^0$ deposition,


https://doi.org/10.1021/acsnano.4c10343
ACS Nano 2024, 18, 32723−32731

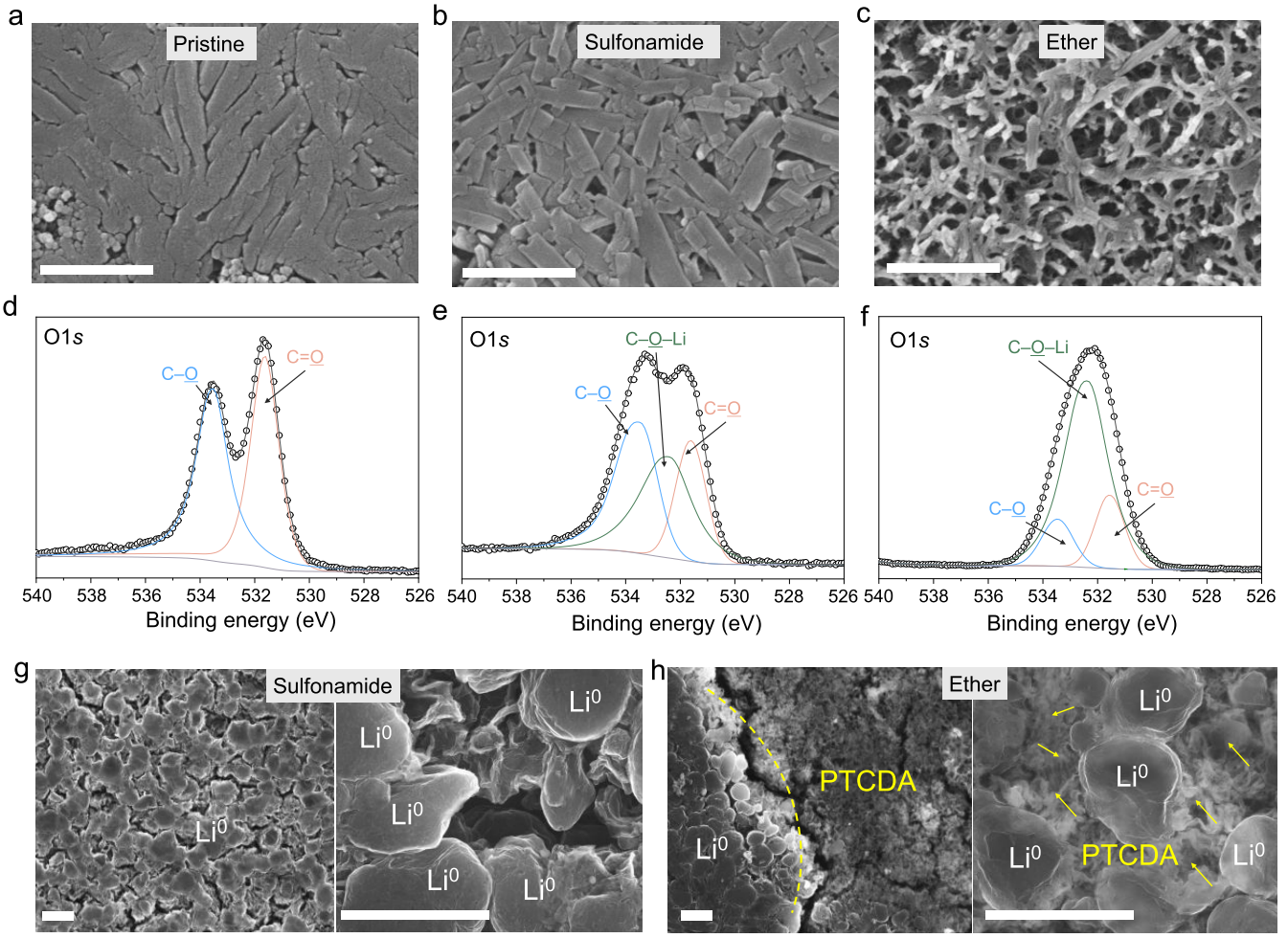


**Figure 4. Postmortem analysis on the cycled PTCDA cathodes and LMAs. SEM images of the pristine PTCDA cathodes (a) and the ones cycled in 1 M LiFSI/DMTMSA (b) and 1 M LiTFSI/DME-DOL-$LiNO_3$ (c) electrolytes for 100 cycles. Scale bars: 1 $\mu$m. (d–f) Surface chemistries revealed by the XPS measurements on the cathodes in parts (a–c). SEM images of the LMAs cycled in 1 M LiFSI/DMTMSA (g) and 1 M LiTFSI/DME-DOL-$LiNO_3$ (h). Scale bars: 10 $\mu$m. The cycled PTCDA cathodes and the LMA foils were extracted from the Li|| PTCDA cells after 100 cycles at the fully charged state. The yellow arrows in part (h) indicate the deposited PTCDA on the LMA surface.**

which is one of the reasons for the poor cycling performance in the ether-based electrolyte.

To gain insight into the phase evolution of the PTCDA in different electrolytes during the discharge–charge process, *ex situ* X-ray diffraction (XRD) was conducted on the Li||PTCDA cells at different SOCs between 1.7 and 3 V (Figure 5a). The reflections of the pristine PTCDA powder and the as-made cathode before cycling were identical (Supporting Information, Figure S5). Upon discharging in the sulfonamide-based electrolyte, the strongest characteristic peak located at 12.35° shifted toward lower angles after Li intercalation (Figure 5b). All characteristic peaks were slightly weakened during the discharge–charge process and recovered to their original intensity at the fully delithiated state, suggesting that only a very small fraction of PTCDA on the surface rather was turned into amorphous or dissolved. In contrast, all of the characteristic peaks of the PTCDA in the ether-based electrolyte disappeared after Li intercalation (Figure 5c), clearly indicating almost all of the PTCDA was dissolved into ethers, which matches well with the visual observation in Figure 3. Such a difference in dissolution behaviors has a great impact on the cell impedance as the dissolved PTCDA RMs can cover the LMA surface and block ion transportation. *In situ* electrochemical impedance spectroscopy (EIS) was performed on the Li||PTCDA cells with different electrolytes at different SOCs (Figure 5d,e). During the lithiation/delithiation of PTCDA in the sulfonamide-based electrolyte, the resistance remained very stable (Figure 5d) while the cell in the ether-based electrolyte exhibited higher resistance before cycling that was increased by a factor of 2 at the full lithiation state and cannot be recovered after full delithiation (Figure 5e). It points to a shuttling phenomenon where some PTCDA RMs formed an irreversible high-impedance SEI on the LMA despite the presence of $LiNO_3$. From the above results and discussions, it is apparent that the dissolution of PTCDA in the electrolyte is greatly suppressed in the sulfonamide-based electrolyte, and thus, the QSSC is successfully realized, which could be mainly attributed to the DMTMSA solvent effect (Supporting Information, Figure S6). Such a QSSC favors fast redox reaction kinetics with high average EEs of ~95.6% and enables excellent cycling stability (~95.8% retention over 300 cycles), much better than the traditional dissolution-involved conversion reaction.

After realizing the QSSC, we can easily calculate the lattice parameters of PTCDA during the Li intercalation–deintercalation process from the XRD patterns (Figure 5b). It indicates a volume change of ~2.64% after Li intercalated into the


https://doi.org/10.1021/acsnano.4c10343
ACS Nano 2024, 18, 32723–32731

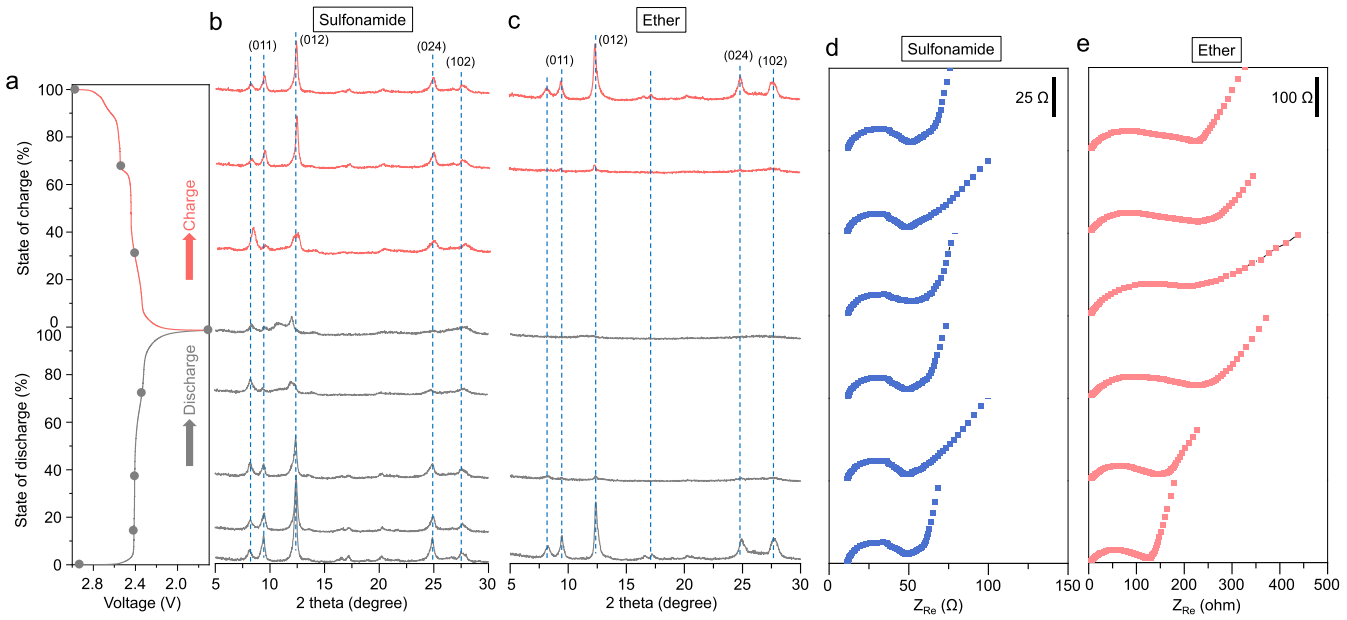


**Figure 5. Phase and impedance evolution during the charging−discharging process in different electrolytes. (a) Voltage profiles of the Li|| PTCDA cell. The gray dots on the profiles correspond to different SOCs for the *ex situ* XRD measurements in the sulfonamide-based (b) and ether-based (c) electrolytes. *In situ* EIS spectra at the same SOCs of the Li||PTCDA cells in the sulfonamide-based (d) and ether-based (e) electrolytes.**

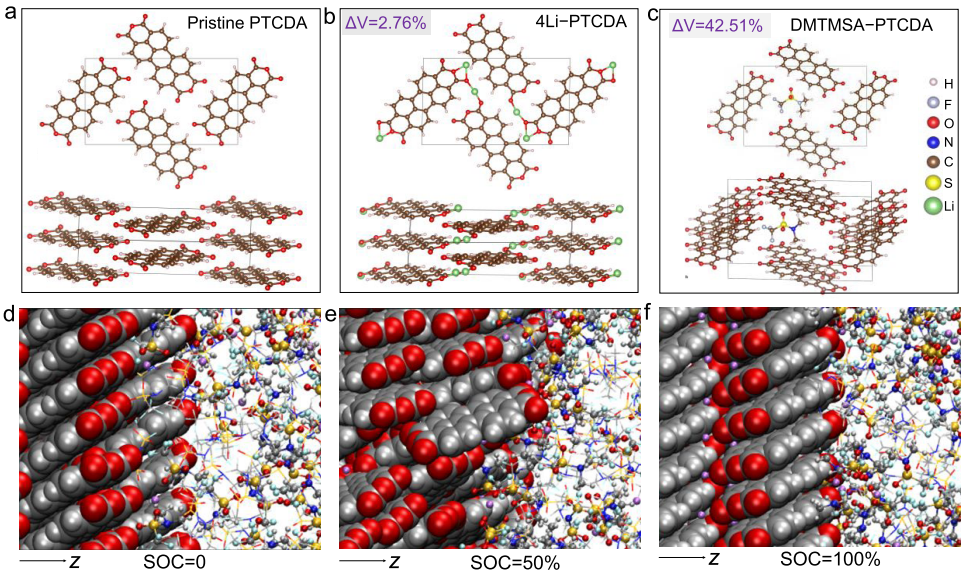


**Figure 6. DFT and MD simulations on the solvent cointercalation mechanism. DFT models of simulated pristine PTCDA and PTCDA with Li intercalation and solvent molecule cointercalation from the top view and the side view. (a) Pristine PTCDA molecules, (b) simulated PTCDA unit cell incorporating four Li atoms, (c) simulated DMTMSA-inserted PTCDA unit cell. MD simulated interfaces between the 1 M LiFSI/DMTMSA electrolyte and the PTCDA at different SOCs simulated. (d) Pristine PTCDA before Li intercalation (SOC = 0), (e) one Li intercalated per one PTCDA molecule (SOC = 50%), and (f) two Li intercalated per one PTCDA molecule (SOC = 100%).**

PTCDA compared to the one before Li intercalation. An important question to be answered is whether the DMTMSA solvent molecule is cointercalated with the $Li^+$ cation into the stacked PTCDA layers or not. To shed more light on this critical issue, first-principles density functional theory (DFT) calculations were performed on the Li-PTCDA-DMTMSA systems (Figure 6 and Supporting Information, Figure S6). The original unit cell was constructed of several stacked PTCDA molecules (Figure 6a). Then, we inserted one, two, four Li atoms, and one DMTMSA molecule into the crevices between the stacked PTCDA molecules, respectively. After full relaxation to an energetically favorable configuration, lattice constants and the volume change after intercalation ($\Delta V$) were calculated (Supplementary Methods and Supporting Information, Table S1). It is apparent that the $\Delta V$ after four Li atoms intercalation is estimated to be 2.76% (Figure 6b), which is close to with the value deduced from the XRD patterns (~2.64%). The substantially large $\Delta V \sim 42.51\%$ after the DMTMSA molecule intercalation implies that the DMTMSA molecule may not be cointercalated into the bulk PTCDA layers. To further elucidate the dissolution within the interface between PTCDA and electrolyte, molecular dynamics (MD)


https://doi.org/10.1021/acsnano.4c10343
ACS Nano 2024, 18, 32723−32731

simulations were conducted according to the reference.[35] PTCDA models at three different states of charge (pristine, SOC = 0; one Li intercalated per one PTCDA molecule, SOC = 50%; and two Li intercalated per one PTCDA molecule, SOC = 100%) were constructed (Supporting Information, Figure S7). The images of the enlarged interfacial regions are shown in Figure 6d–f. At SOC = 0, the interface between PTCDA and electrolyte molecules is distinguishable (Figure 6d), and the PTCDA molecules are uniformly distributed within ±3 nm (Supporting Information, Figure S8a). At SOC = 50%, the crystal structure of PTCDA exhibits slight disorder due to the asymmetry after Li is intercalated (Figure 6e). The PTCDA–electrolyte interface shows some interactive disturbance with ∼1 nm away toward the electrolyte region (Supporting Information, Figure S8b) compared to that at SOC = 0, revealing slight dissolution behavior. The PTCDA at the fully discharged state (SOC = 100%) is quite similar to that at SOC = 0, with an increase in the symmetry of the molecular structure (Figure 6f, Supporting Information, Figure S8c). These simulations suggest that DMTMSA cointercalation behavior unlikely occur in the PTCDA bulk but could be present in the interfacial area.

## CONCLUSIONS

By rationally designing a sulfonamide-based electrolyte, 1 M LiFSI/DMTMSA, the QSSC in the PTCDA cathode was successfully enabled. The weakly solvated capability of the DMTMSA-based electrolyte effectively inhibited the historically problematic dissolution of PTCDA at different SOCs, which favors the crystalline phase transition and uniform Li-metal deposition. Benefiting from the QSSC, the Li||PTCDA cell reached a high capacity retention of ∼95.8% after 300 cycles in our sulfonamide-based electrolyte, compared to only ∼60.9% retention over 200 cycles in the ether-based electrolyte. A high and stable energy efficiency of ∼95% over 300 cycles was also achieved in our electrolyte, demonstrating an intrinsic faster kinetics for the QSSC of the PTCDA cathode than the traditional dissolution-involved reaction in the ether-based electrolyte. The DFT calculations and MD simulations implied that the DMTMSA solvent cointercalation may be present at the PTCDA–electrolyte interface but unlikely occurs in the PTCDA bulk. This work overcomes the major challenge associated with the dissolution of PTCDA in electrolytes and develops electrolytes for highly stable and efficient Li–organic batteries.

## METHODS

**Materials.** Perylene-3,4,9,10-tetracarboxylic dianhydride (PTCDA) powder was purchased from Macklin Co. Conductive carbon (Super C45), LiFSI, poly(vinylidene difluoride) (PVDF), *N*-methyl-2-pyrrolidone (NMP), 1 M LiTFSI in DME-DOL 1:1 (v) with 2% $LiNO_3$, and Li-metal foils were purchased from Canrd Co. DMTMSA solvent was synthesized according to our previous work.[26] All solvents were immersed into 5 Å molecular sieves for 3 days to remove residual water before use. Molarity (M, mole salt in liter solution, in mol $L^{-1}$) denotes the electrolyte salt concentration.

**Electrochemical Performances.** For the PTCDA electrodes, a slurry was prepared by mixing PTCDA (70%), Super C45 (20%), and PVDF (10%) in NMP. The slurry was then cast onto carbon-coated aluminum foil and dried at 120 °C for 10 h under vacuum, followed by rolling and punching into round disks with 10 mm diameter. The areal mass loading of active materials is ∼2 mg $cm^{-2}$. CR2032 coin cells were prepared using PTCDA as the cathode, Celgard 2320 as the separator, and Li-metal foil as the anode in the glovebox with $O_2$ and $H_2O$ levels <0.1 ppm. The volume of electrolytes per coin cell was controlled to ∼20 μL by pipets. Landt CT-3002A and Neware CT-4008Tn cyclers were used to perform galvanostatic cycling at different C rates (1C = 130 mA $g^{-1}$). GITT test was performed between 1.7 and 3.0 V with current pulse intervals at ∼0.5C for 8 min, followed by 60 min rests. *In situ* EIS was performed on a Solartron XM-studio electrochemical station at different SOCs.

**Characterizations.** Cycled Li and PTCDA electrodes were obtained by disassembling coin cells in the glovebox and then washing them thoroughly with DME and dimethyl carbonate to remove residual lithium salts, respectively. The dissolution of RMs in different electrolytes was measured with UV–vis (PE Lambda950). The morphology and microstructure of the PTCDA cathodes and LMAs before and after cycling were examined by high-resolution SEM (HITACHI SU6600). The surface chemistry of the cycled electrodes was analyzed by XPS (Thermo Fisher ESCALAB Xi+). The phase compositions of the PTCDA cathodes at different SOCs were *ex situ* collected by XRD (Bruker D8 ADVANCE). The samples for the *ex situ* XRD measurements were made by the following steps to increase the XRD intensity. Bare Al foil was used to replace the carbon-coated Al foil to reduce adhesion. After slurry coating, drying, and punching, the electrodes were rolled at a higher pressure than normal. Then, the active material layer was carefully peeled off of the Al foil, which was used to make samples at different SOCs and XRD measurements.

**Calculations.** First-principles calculations were performed using the Vienna ab initio simulation package (VASP) based on density functional theory.[36,37] The projected augmented wave (PAW) was used to describe the interaction energy between ions and electrons,[38] and the generalized gradient approximation (GGA) of the Perdew–Burke–Ernzerhof (PBE) function was used to describe the exchange-correlation energy.[39] In the calculations, we considered spin polarization, and the DFT-D3 method was adopted for the van der Waals correction.[40] In the structure relaxation convergence process of the material model, we set the plane wave cutoff energy to 450 eV and adopted the convergence standard of $10^{-4}$ eV for the energy. The γ-centered Monkhorst-Pack *k*-points mesh with a density of 0.04 $Å^{-1}$ for structural relaxation was used to sample the Brilliouin zone.[41] Considering that sufficient space between PTCDA molecules is required for the entry of solvent molecules, the original cell was scaled by 1.2 times equal ratio to expand the space in the cell, and it was optimized to obtain a pristine unit cell, and then one DMTMSA molecule was inserted into the expanded cell, and one Li, two, and four Li atoms were, respectively, inserted into the pristine unit cell, and the structure relaxation was carried out, respectively. Lattice constants including *a*, *b*, *c*, *α*, *β*, *γ* and the volume of unit cell V were deduced from the relaxed unit cells. Δ*V* values were calculated by the cell volume after intercalation divided by the pristine cell volume before intercalation. The molecular dynamics (MD) simulation of this interface system between PTCDA at three different SOCs and electrolyte solutions were carried out using the Gromacs program suite.[42] The $Li^+/FSI^-$ and the DMTMSA molecules were simulated using CL&P force field parameters[43] and the OPLS-AA/M force field,[44] respectively. The neutral PTCDA crystal and lithium-intercalated PTCDA crystals in which the PTCDA molecules have one and two negative charges were also simulated using the Lennard-Jones parameters of the OPLS-AA/M force field and the RESP atomic charge calculated through DFT calculations. All of these topology files for MD simulation were generated using the auxiliary tools of force field (AuToFF) web server.[45] In order to construct the electrode–electrolyte interface models, the initial simulation boxes containing 240 PTCDA molecules were constructed from the crystal structure file. A vacuum layer of 15 nm thickness was added in the *c*-direction of the model, and then, the lithium cation, FSI anions, and DMTMSA solvent molecules were inserted according to the real mole ratio of our electrolyte. These structures were first energy-minimized and then annealed from 400 to 298.15 K over a 1 ns time period, with a time step of 1 ps, to reach an equilibrium state. The temperature was maintained at 298.15 K using the velocity-rescale thermostat[46] with a relaxation constant of 1 ps. The pressure was maintained at 1.01325 × $10^5$ Pa using Berendsen's barostat with a semi-isothermal compres-


https://doi.org/10.1021/acsnano.4c10343
ACS Nano 2024, 18, 32723–32731

sibility constant of 4.5 × $10^{-5}$ along the *z*-axis. Periodic boundary conditions were applied in all directions, and the electrostatic interactions and van der Waals forces were treated using the Particle-mesh Ewald (PME) method with a cutoff distance of 15 Å. Following the energy-minimization and -equilibration steps, a 20 ns MD simulation was performed, with the trajectory saved every 1 ps. The interactions between the electrode molecules and solution molecules were calculated by rerunning the exported trajectories of isolated components and complex components using Gromacs tool suites.

## ASSOCIATED CONTENT

### Data Availability Statement

All data are available in the main text or the Supporting Information.

### Supporting Information

The Supporting Information is available free of charge at https://pubs.acs.org/doi/10.1021/acsnano.4c10343.

The color evolution, SEM figures, XRD spectra, supplementary electrochemical performance, and supplementary simulation details (PDF)

## AUTHOR INFORMATION


### Corresponding Authors

**Chuanjin Tian** − *School of Materials Science and Engineering, Jingdezhen Ceramic University, Jingdezhen 333001, China*; Email: tianchuanjin@jci.edu.cn

**Weijiang Xue** − *Center for Advancing Materials Performance from the Nanoscale (CAMP-Nano), State Key Laboratory for Mechanical Behavior of Materials, Xi'an Jiaotong University, Xi'an 710049, China*; orcid.org/0000-0002-3060-4580; Email: xuewj@xjtu.edu.cn

### Authors

**Huang Cai** − *Center for Advancing Materials Performance from the Nanoscale (CAMP-Nano), State Key Laboratory for Mechanical Behavior of Materials, Xi'an Jiaotong University, Xi'an 710049, China*

**Xinke Cui** − *Center for Advancing Materials Performance from the Nanoscale (CAMP-Nano), State Key Laboratory for Mechanical Behavior of Materials, Xi'an Jiaotong University, Xi'an 710049, China*

**Yonghao Shi** − *School of Materials Science and Engineering, Jingdezhen Ceramic University, Jingdezhen 333001, China*

**Yuxin Zhang** − *School of Energy and Power Engineering, Xi'an Jiaotong University, Xi'an 710049, China*

**Xinran Chen** − *School of Energy and Power Engineering, Xi'an Jiaotong University, Xi'an 710049, China*

**Linghan Fan** − *The Second Affiliated Hospital of Xi'an Jiaotong University, Xi'an 710004, China*

**Jian Zhou** − *Center for Alloy Innovation and Design, State Key Laboratory for Mechanical Behavior of Materials, Xi'an Jiaotong University, Xi'an 710049, China*; orcid.org/0000-0002-2606-4833

Complete contact information is available at: https://pubs.acs.org/10.1021/acsnano.4c10343


### Author Contributions

W.X. and H.C. conceived the concept. W.X. designed the electrolyte and led the project. H.C., X.K.C., Y.Z., X.R.C., and L.F. conducted electrochemical measurements. H.C. conducted UV−vis spectra and *in situ* EIS measurements. H.C. and X.K.C. conducted *ex situ* XRD measurements and SEM analysis. H.C. conducted XPS measurements and analyzed the results with W.X. Y.S., C.T., and J.Z. conducted the calculations. W.X., H.C., and C.T. wrote and revised the manuscript. All authors discussed the results and reviewed the manuscript.

### Notes

The authors declare no competing financial interest.

## ACKNOWLEDGMENTS

The authors would like to acknowledge the support of the startup project from Xi'an Jiaotong University and the National Training Program of Innovation for Undergraduates (XJ202310698060). The authors would also like to acknowledge Chenyu Liang and Fuchun Tan at the Instrumental Analysis Center of Xi'an Jiaotong University for their assistance with XPS, XRD, and UV−vis analyses.

## REFERENCES


(1) Lyu, H.; Sun, X.-G.; Dai, S. Organic Cathode Materials for Lithium-Ion Batteries: Past, Present, and Future. *Adv. Energy Sustainability Res.* **2021**, *2*, No. 2000044.

(2) Eui-Hyurk, N.; Youngoh, K.; Sang-Jin, J.; Ye-Jin, A.; Yun-Jung, L.; Yun-Chae, J.; Joonmyung, C.; Won-Jin, K. Pre-impregnated Protective Layer for High Energy Density Li Metal Batteries Using Aqueous Electrolyte. *Chem. Eng. J.* **2024**, *15*, No. 151269.

(3) Gwanghyeon, C.; Youngoh, K.; Joonmyung, C.; Duho, K. Thermodynamic Factor for Facilitating Homogeneous Dendrite Growth in Alkali Metal Batteries. *Adv. Energy Mater.* **2022**, *12*, No. 2201428.

(4) Choi, J. U.; Voronina, N.; Sun, Y. K.; Myung, S. T. Recent Progress and Perspective of Advanced High-Energy Co-Less Ni-Rich Cathodes for Li-Ion Batteries: Yesterday, Today, and Tomorrow. *Adv. Energy Mater.* **2020**, *10*, No. 2002027.

(5) Han, X.; Chang, C.; Yuan, L.; Sun, T.; Sun, J. Aromatic Carbonyl Derivative Polymers As High-Performance Li-Ion Storage Materials. *Adv. Mater.* **2007**, *19*, 1616−1621.

(6) Karlsmo, M.; Bouchal, R.; Johansson, P. High-Performant All-Organic Aqueous Sodium-Ion Batteries Enabled by PTCDA Electrodes and a Hybrid Na/Mg Electrolyte. *Angew. Chem., Int. Ed.* **2021**, *60*, 24709−24715.

(7) Zhang, W.; Sayavong, P.; Xiao, X.; Oyakhire, S. T.; Shuchi, S. B.; Vilá, R. A.; Boyle, D. T.; Kim, S. C.; Kim, M. S.; Holmes, S. E.; et al. Recovery of Isolated Lithium through Discharged State Calendar Ageing. *Nature* **2024**, *626*, 306−312.

(8) Pang, Q.; Shyamsunder, A.; Narayanan, B.; Kwok, C. Y.; Curtiss, L. A.; Nazar, L. F. Tuning the Electrolyte Network Structure to Invoke Quasi-Solid State Sulfur Conversion and Suppress Lithium Dendrite Formation in Li-S Batteries. *Nat. Energy* **2018**, *3*, 783−791.

(9) Xue, W.; Yan, Q.-B.; Xu, G.; Suo, L.; Chen, Y.; Wang, C.; Wang, C.-A.; Li, J. Double-Oxide Sulfur Host for Advanced Lithium-Sulfur Batteries. *Nano Energy* **2017**, *38*, 12−18.

(10) Xue, W.; Miao, L.; Qie, L.; Wang, C.; Li, S.; Wang, J.; Li, J. Gravimetric and Volumetric Energy Densities of Lithium-Sulfur Batteries. *Curr. Opin. Electrochem.* **2017**, *6*, 92−99.

(11) Xue, W.; Yu, D.; Suo, L.; Wang, C.; Wang, Z.; Xu, G.; Xiao, X.; Ge, M.; Ko, M.; Chen, Y.; et al. Manipulating Sulfur Mobility Enables Advanced Li-S Batteries. *Matter* **2019**, *1*, 1047−1060.

(12) Xue, W.; Shi, Z.; Suo, L.; Wang, C.; Wang, Z.; Wang, H.; So, K. P.; Maurano, A.; Yu, D.; Chen, Y.; et al. Intercalation-Conversion Hybrid Cathodes Enabling Li-S Full-Cell Architectures with Jointly Superior Gravimetric and Volumetric Energy Densities. *Nat. Energy* **2019**, *4*, 374−382.

(13) Han, Y.; Ning, W.; Du, H.; Yang, J.; Wang, N.; Cao, L.; Li, F.; Zhang, F.; Xu, F.; Tian, M. Preparation, Optical and Electrical Properties of PTCDA Nanostructures. *Nanoscale* **2015**, *7*, 17116−17121.

(14) Lu, Y.; Chen, J. Prospects of Organic Electrode Materials for Practical Lithium Batteries. *Nat. Rev. Chem.* **2020**, *4*, 127−142.
(15) Guo, H.; Elmanzalawy, M.; Sivakumar, P.; Fleischmann, S. Unifying Electrolyte Formulation and Electrode Nanoconfinement Design to Enable New Ion−Solvent Cointercalation Chemistries. *Energy Environ. Sci.* **2024**, *17*, 2100−2116.
(16) Qin, M.; Zeng, Z.; Wu, Q.; Yan, H.; Liu, M.; Wu, Y.; Zhang, H.; Lei, S.; Cheng, S.; Xie, J. Dipole−Dipole Interactions for Inhibiting Solvent Co-Intercalation into a Graphite Anode to Extend the Horizon of Electrolyte Design. *Energy Environ. Sci.* **2023**, *16*, 546−556.
(17) Jache, B.; Adelhelm, P. Use of Graphite As a Highly Reversible Electrode with Superior Cycle Life for Sodium-Ion Batteries by Making Use of Co-Intercalation Phenomena. *Angew. Chem., Int. Ed.* **2014**, *53*, 10169−10173.
(18) Park, J.; Xu, Z. L.; Yoon, G.; Park, S. K.; Wang, J.; Hyun, H.; Park, H.; Lim, J.; Ko, Y. J.; Yun, Y. S.; Kang, K. Stable and High-Power Calcium-Ion Batteries Enabled by Calcium Intercalation into Graphite. *Adv. Mater.* **2020**, *32*, No. 1904411.
(19) Wei, Z.; Shin, W.; Jiang, H.; Wu, X.; Stickle, W. F.; Chen, G.; Lu, J.; Alex Greaney, P.; Du, F.; Ji, X. Reversible Intercalation of Methyl Viologen as a Dicationic Charge Carrier in Aqueous Batteries. *Nat. Commun.* **2019**, *10*, No. 3227.
(20) Mao, M.; Wang, S.; Lin, Z.; Liu, T.; Hu, Y. S.; Li, H.; Huang, X.; Chen, L.; Suo, L. Electronic Conductive Inorganic Cathodes Promising High-Energy Organic Batteries. *Adv. Mater.* **2021**, *33*, No. 2005781.
(21) Wei, C.; Tan, L.; Zhang, Y.; Xi, B.; Xiong, S.; Feng, J. MXene/Organics Heterostructures Enable Ultrastable and High-Rate Lithium/Sodium Batteries. *ACS Appl. Mater. Interfaces* **2022**, *14*, 2979−2988.
(22) Belanger, R. L.; Commarieu, B.; Paolella, A.; Daigle, J. C.; Bessette, S.; Vijh, A.; Claverie, J. P.; Zaghib, K. Diffusion Control of Organic Cathode Materials in Lithium Metal Battery. *Sci. Rep.* **2019**, *9*, No. 1213.
(23) Zhang, Q.; Zhang, Y.; Wei, C.; An, Y.; Tan, L.; Xiong, S.; Feng, J. Highly Reversible Lithium Metal-Organic Battery Enabled by a Freestanding MXene Interlayer. *J. Power Sources* **2022**, *521*, No. 230963.
(24) Cai, T.; Han, Y.; Lan, Q.; Wang, F.; Chu, J.; Zhan, H.; Song, Z. Stable Cycling of Small Molecular Organic Electrode Materials Enabled by High Concentration Electrolytes. *Energy Storage Mater.* **2020**, *31*, 318−327.
(25) Sieuw, L.; Jouhara, A.; Quarez, E.; Auger, C.; Gohy, J. F.; Poizot, P.; Vlad, A. A H-Bond Stabilized Quinone Electrode Material for Li-Organic Batteries: the Strength of Weak Bonds. *Chem. Sci.* **2019**, *10*, 418−426.
(26) Chen, S.; Zheng, J.; Mei, D.; Han, K. S.; Engelhard, M. H.; Zhao, W.; Xu, W.; Liu, J.; Zhang, J.-G. High-Voltage Lithium-Metal Batteries Enabled by Localized High-Concentration Electrolytes. *Adv. Mater.* **2018**, *30*, No. 1706102.
(27) Wang, M.; Liu, T.; Du, X.; Sun, Y.; Wang, L.; Zhang, Z.; Wang, X.; Cui, G. Weakening Solvent Polarity Enables Shuttle-Effect-Free and Temperature-Independent Lithium-Organic Batteries. *Energy Storage Mater.* **2023**, *60*, No. 102816.
(28) Xue, W.; Huang, M.; Li, Y.; Zhu, Y. G.; Gao, R.; Xiao, X.; Zhang, W.; Li, S.; Xu, G.; Yu, Y.; et al. Ultra-High-Voltage Ni-Rich Layered Cathodes in Practical Li Metal Batteries Enabled by a Sulfonamide-Based Electrolyte. *Nat. Energy* **2021**, *6*, 495−505.
(29) Xue, W.; Gao, R.; Shi, Z.; Xiao, X.; Zhang, W.; Zhang, Y.; Zhu, Y. G.; Waluyo, I.; Li, Y.; Hill, M. R.; et al. Stabilizing Electrode−Electrolyte Interfaces to Realize High-Voltage Li||$LiCoO_2$ Batteries by a Sulfonamide-Based Electrolyte. *Energy Environ. Sci.* **2021**, *14*, 6030−6040.
(30) Wang, C.; Thenuwara, A. C.; Luo, J.; Shetty, P. P.; McDowell, M. T.; Zhu, H.; Posada-Perez, S.; Xiong, H.; Hautier, G.; Li, W. Extending the Low-Temperature Operation of Sodium Metal Batteries Combining Linear and Cyclic Ether-Based Electrolyte Solutions. *Nat. Commun.* **2022**, *13*, No. 4934.
(31) Zhang, S. S. Role of $LiNO_3$ in Rechargeable Lithium/Sulfur Battery. *Electrochim. Acta* **2012**, *70*, 344−348.
(32) Li, W.; Erickson, E. M.; Manthiram, A. High-Nickel Layered Oxide Cathodes for Lithium-Based Automotive Batteries. *Nat. Energy* **2020**, *5*, 26−34.
(33) Gu, C.; Liu, Z.; Gao, X.; Zhang, Q.; Zhang, Z.; Liu, Z.; Wang, C. Polymerization Increasing the Capacitive Charge Storage for Better Rate Performance: A Case Study of Electrodes in Aqueous Sodium-Ion Capacitors. *Battery Energy* **2022**, *1*, No. 20220031.
(34) Hobold, G. M.; Lopez, J.; Guo, R.; Minafra, N.; Banerjee, A.; Shirley Meng, Y.; Shao-Horn, Y.; Gallant, B. M. Moving Beyond 99.9% Coulombic Efficiency for Lithium Anodes in Liquid Electrolytes. *Nat. Energy* **2021**, *6*, 951−960.
(35) Hyun-Wook, L.; Youngoh, K.; Joo-Eun, K.; Ja-Yeong, K.; Jae-Yeon, J.; Joonmyung, C.; Won-Jin, K. Diluents Effect on Inhibiting Dissolution of Organic Electrode for Highly Reversible Li-Ion Batteries. *Adv. Energy Mater.* **2024**, *14*, No. 2303033.
(36) Kresse, G.; Furthmuller, J. Efficient Iterative Schemes for Ab Initio Total-Energy Calculations Using a Plane-Wave Basis Eet. *Phys. Rev. B* **1996**, *54*, 11169−11186.
(37) Kresse, G.; Furthmuller, J. Efficiency of Ab-Initio Total Energy Calculations for Metals and Semiconductors Using a Plane-Wave Basis Set. *Comput. Mater. Sci.* **1996**, *6*, 15−50.
(38) Blöchl, P. E. Projector Augmented-Wave Method. *Phys. Rev. B* **1994**, *50*, 17953−17979.
(39) Perdew, J. P.; Burke, K.; Ernzerhof, M. Generalized Gradient Approximation Made Simple. *Phys. Rev. Lett.* **1996**, *77*, 3865−3868.
(40) Grimme, S.; Antony, J.; Ehrlich, S.; Krieg, H. A Consistent and Accurate Ab Initio Parametrization of Density Functional Dispersion Correction (DFT-D) for the 94 Elements H-Pu. *J. Chem. Phys.* **2010**, *132*, No. 154104.
(41) Monkhorst, H. J.; Pack, J. D. Special Points for Brillouin-Zone Integrations. *Phys. Rev. B* **1976**, *13*, 5188−5192.
(42) Abraham, M. J.; Murtola, T.; Schulz, R.; Páll, S.; Smith, J. C.; Hess, B.; Lindahl, E. GROMACS: High Performance Molecular Simulations Through Multi-Level Parallelism from Laptops to Supercomputers. *SoftwareX* **2015**, *1−2*, 19−25.
(43) Lopes, J. N. C.; Pádua, A. A. CL&P: A Generic and Systematic Force Field for Ionic Liquids Modeling. *Theor. Chem. Acc.* **2012**, *131*, 1129.
(44) Robertson, M. J.; Qian, Y.; Robinson, M. C.; Tirado-Rives, J.; Jorgensen, W. L. Development and Testing of the OPLS-AA/M Force Field for RNA. *J. Chem. Theory Comput.* **2019**, *15*, 2734−2742.
(45) Wang, C.; Li, W.; Liao, K.; Wang, Z.; Wang, Y.; Gong, K. *AuToFF Program*, version 1.0; Hzwtech: Shanghai, 2023. https://cloud.hzwtech.com/web/product-service?id=36.
(46) Bussi, G.; Donadio, D.; Parrinello, M. Canonical Sampling Through Velocity Rescaling. *J. Chem. Phys.* **2007**, *126*, No. 014101.


https://doi.org/10.1021/acsnano.4c10343
*ACS Nano* 2024, 18, 32723−32731